

PAPER • OPEN ACCESS

Minimizing the linewidth enhancement factor in multiple-quantum-well semiconductor optical amplifiers

To cite this article: Özüm Emre Aşırım and Christian Jirauschek 2022 *J. Phys. B: At. Mol. Opt. Phys.* **55** 115401

View the [article online](#) for updates and enhancements.

You may also like

- [Application of a large wall electric probe \(LWEP\) for plasma and ambient gas studies](#)
V I Demidov, S F Adams and I P Kurlyandskaya
- [Bridging the gap between the water-energy-food nexus and compound risks](#)
J Leah Jones-Crank, Jessie Lu and Ben Orlove
- [Stakeholder perspectives on fostering the water-energy-food nexus in Jordan: lessons beyond agricultural water management](#)
Abel Chemura, Walaa Al-Smadi, Ali Abkar et al.

Minimizing the linewidth enhancement factor in multiple-quantum-well semiconductor optical amplifiers

Özüm Emre Aşırım*  and Christian Jirauschek 

Department of Electrical and Computer Engineering, Technical University of Munich, Arcisstrasse 21, 80333 Munich, Germany

E-mail: ozum.asirim@tum.de and jirauschek@tum.de

Received 20 February 2022, revised 20 April 2022

Accepted for publication 26 April 2022

Published 17 May 2022



CrossMark

Abstract

Semiconductor optical amplifiers (SOAs) often exhibit pronounced phase noise owing to their inherently high linewidth enhancement factor (LWEF). The signal to noise ratio of a SOA is often decreased due to refractive index fluctuations in the gain medium causing distorted phase relationship between the generated photons, which is quantified by the LWEF. A simple and precise theoretical model that offers a prescription for minimizing the LWEF in SOAs is unavailable in the literature. In this study, we have developed an inclusive yet simple algorithmic model that aims to both represent the variation and to provide a strategy for minimizing the LWEF in multiple-quantum-well (MQW) based SOAs. The results of the presented model were verified via a reasonable agreement with experimental results. This study provides a theoretical description of how to adjust the LWEF through tuning of the most critical MQW SOA parameters in the design stage.

Keywords: semiconductor optical amplifier, linewidth enhancement factor, multiple quantum well, intraband collision, FDML


(Some figures may appear in colour only in the online journal)

1. Introduction

Semiconductor optical amplifiers (SOAs) are compact photonic devices for light amplification based on the stimulated emission phenomenon. SOAs typically provide an optical gain factor up to 30 dB within a gain bandwidth of 10 to 30 THz in the near infra-red region (around 1300 nm) [1, 2]. They are very useful in integrated photonic devices that are applied in optical communications and optical data processing. This is attributed to their compactness, rapid optical response, and relatively large gain-bandwidth product [3–10]. Appreciable

research has been done to enhance the gain-bandwidth product of SOAs [4–11]. The gain of SOAs is known to be intertwined with *linewidth enhancement* (LWE) due to refractive index fluctuations within the gain bandwidth, which is quantified by a parameter called the *linewidth enhancement factor* (LWEF) [12–25]. Therefore, in the context of enhancing the gain-bandwidth product of SOAs, taking the LWEF of SOAs into consideration is a must to account for the enhanced phase noise that distorts the output signal [18–25]. One example is the case of *Fourier domain mode locked lasers* where SOA partakes as the most critical element, and the sharp variation of the LWEF introduces significant phase noise in the output intensity pattern [3, 26, 27]. Currently, the LWEF of SOAs ranges from 1 to 8 for multiple quantum-well (MQW) based SOAs, and from 5 to 20 in SOAs with bulk active media, which leads to a drastic decrease in signal to noise ratio due to the

* Author to whom any correspondence should be addressed.

 Original content from this work may be used under the terms of the [Creative Commons Attribution 4.0 licence](https://creativecommons.org/licenses/by/4.0/). Any further distribution of this work must maintain attribution to the author(s) and the title of the work, journal citation and DOI.

enhancement of the phase-noise [11–15]. Prominent results in the literature of SOA–LWEF are mostly experimental, especially for MQW based gain media [28–38]. It is not known for sure how the LWEF of SOAs can be precisely and accurately decreased via a precise tuning of the SOA parameters in a particular manner. There is also disagreement among different experimental observations and among the few available theoretical studies [8–41]. It is widely accepted that the gain enhancement in MQW-based active media (via carrier confinement) decreases the LWEF. However, a convenient algorithmic model that accurately quantifies the variation of the LWEF with respect to the variation of the SOA parameters is lacking.

To minimize the LWEF, its main culprit, which is the fluctuations of the refractive index, must be minimized [37–41]. Therefore, in this study, all parameters that influence the refractive index are investigated to provide a systematic approach in decreasing the LWEF of MQW SOAs. Concerning the effect of carrier confinement, both the SOAs with a bulk active region and the ones with a MQW based active region are investigated for comparison. Emphasis is put on the influence of the intraband collision rate under quantum confinement, which is believed to be a major determinant of the LWEF [39].

For an efficient stimulated emission process, the phase relationship between the generated photons must be precise and free from distortion. On the other hand, to achieve a high gain factor, the carrier concentration must be high, which makes the refractive index fluctuate more and inevitably induce phase distortion, thereby decreasing the efficiency of the stimulated emission process. Hence, the attainment of a higher SOA gain factor via an increase of the electrical pump current is associated with a higher phase noise due to greater refractive index fluctuations [9–15].

To reduce these refractive index fluctuations, carrier confinement is essential. Due to the energy levels being discrete in quantum wells (QWs), carriers can be effectively confined. The confinement of carriers means a higher rate of intraband collisions, leading to the spatial distribution of the electrons and holes becoming more deterministic. Conversely, a lower intraband collision rate means more impactful collisions and the spatial distributions becoming more randomized. This random spatial distribution of the electrons/holes induces fluctuations in the refractive index as the spatial distribution evolves over time [42–45]. For this reason, the intraband collision rate is of particular importance in the evaluation of the LWEF and will be a subject of focus in this study.

To model the LWEF of SOAs, firstly, the semiconductor electron dynamics is modeled using the rate equations for the electron and photon densities, along with the distribution of energy levels and the corresponding occupation probabilities for conduction and valence bands. The instantaneous photon density, carrier concentrations, and the SOA small-signal gain are determined by solving the rate equations. As the instantaneous electron/hole concentrations are evaluated, fluctuations in the refractive index can be computed through the formulation of the permittivity term based on the distribution of energy levels and the corresponding occupation probabilities, which influences the LWEF and the SOA dynamics through inducing

fluctuations in carrier lifetime, optical confinement factor, and the intraband collision time. The next step involves the evaluation of the real and imaginary parts of the electric susceptibility and their derivatives with respect to the carrier density. The ratio of the derivatives of the real and imaginary parts of the electric susceptibility yields the LWEF [37, 42]. Since the evaluation of the electric susceptibility requires the knowledge of the density of states and the occupation probabilities, a precise determination of the conduction and valence band Fermi energies is needed in quasi thermal-equilibrium based on the electron and hole concentrations. The density of states naturally depends on whether the SOA gain medium is a bulk or an MQW-based active medium, which, in the case of an MQW-based gain medium, also depends on the width of each well. Once the LWEF is evaluated for a given set of SOA parameters, its variation will be computationally investigated as a function of the intraband collision time, carrier density, and the lasing frequency. Finally, an ultimate scenario on the minimization of the LWEF will be derived from these computations for MQW SOAs along with a comparison with bulk SOAs.

2. Methods

The LWEF (α) of a laser is approximated as the ratio of the change in the refractive index of the gain medium to the change in carrier density, divided by the ratio of the change in the gain factor to the change in carrier density. This is mathematically expressed as [44]

$$\alpha \approx -\frac{4\pi}{\lambda} \frac{\frac{\partial n_r}{\partial N}}{\frac{\partial g}{\partial N}} = -\frac{4\pi}{\lambda} \frac{\Delta n_r}{\Delta g}, \quad N : \text{carrier density}, \quad g : \text{gain},$$

$$n_r : \text{refractive index}, \quad \lambda : \text{wavelength.} \quad (1)$$

Equation (1) simply states that the cause of the LWE is the change in the refractive index of the gain medium. This change in refractive index depends on the dispersion characteristics of the gain medium, mainly the resonances of absorption and emission, and their associated bandwidth. During the amplification of a laser beam, fluctuating changes in the refractive index randomizes the phase relationship between the emitted photons and warps the coherence of the stimulated emission process. A critical process that strongly affects the LWEF of a laser is the intraband collision of the carriers. When the intraband collision rate is low, the phase relationship between the generated photons is more intensely and more instantaneously disturbed. This is because the carriers have more time to accelerate due to electrical and/or thermal excitation, causing each collision to occur at a greater speed. As the intraband collision rate gets higher, carriers have less time to accelerate between subsequent collisions and the collisions occur at a lower impact or momentum, rendering them less critical [43]. Therefore, in a gain medium where the intraband collision rate is high, phase distortion is largely prevented, which leads to a lower LWEF [39].

The LWEF defined in equation (1) can also be expressed in terms of the ratio of the derivatives of the real and imaginary parts of the electric susceptibility with respect to the carrier

density [13]

$$\alpha(\omega_L, N, T_c) = -\frac{\partial X_R}{\partial X_{IM}}. \quad (2)$$

The real and imaginary susceptibility terms can be concisely expressed in terms of the density of states and the occupation probabilities as [39]

$$X_R = \int_{-\infty}^{\infty} \rho(\omega) A [P_c(N, \omega) - P_v(N, \omega)] \frac{\omega_L - \omega}{(\omega_L - \omega)^2 + T_c^{-2}} d\omega \quad (3)$$

$$X_{IM} = \int_{-\infty}^{\infty} \rho(\omega) A [P_c(N, \omega) - P_v(N, \omega)] \frac{T_c^{-1}}{(\omega_L - \omega)^2 + T_c^{-2}} d\omega \quad (4)$$

$\rho(\omega)$: density of states, ω : angular frequency,

N : carrier density

P_c : occupation probability of electrons in the conduction band

P_v : occupation probability of holes in the valence band

ω_L : angular lasing frequency

T_c : intraband collision time,

A : dipole matrix element dependent coefficient.

(5)

If one computationally examines equations (2)–(4), one can see that there is a strong dependency of the LWEF (α) on the intraband collision time T_c . Figure 1 illustrates the variation of the LWEF for a bulk InP–InGaAsP SOA based on the parameters given in [44]. It is evident that the decrease in the intraband collision time leads to a sharp decrease in the LWEF. This is expected, as the intraband collisions of the carriers lead to phase interruptions for the propagating laser beam inside an SOA waveguide (WG) that would generate *phase noise* through refractive index fluctuations [37–39]. Due to this strong effect of the intraband collisions on the LWEF, the next subsection is dedicated to a more detailed investigation of this phenomenon.

2.1. Intraband collision time

One of the most critical parameters that is involved in the computation of the LWEF is the intraband collision time, which is the duration between two subsequent carrier collisions. The intraband collision time T_c is known to be inversely proportional to the density of electrons/holes in the active region for bulk SOAs, $T_{c,bulk} = \frac{K}{N}$, where N is the carrier density and K is a constant [46–48]. This suggests that under the same excitation parameters and number of carriers, a bulk SOA with a large active medium cross-section (see figure 2) will have a higher carrier collision time compared to an SOA with a smaller active medium cross-section.

For MQW-based SOAs, an elaborate analysis on the intraband carrier collision time is available using *Fermi's golden rule*, based on which it is found that the carrier collision time in a QW is inversely proportional to the carrier density within the wells [47, 48]

$$T_C = \frac{K}{N_{QW}}. \quad (6)$$

Based on this relation between the carrier density and the collision time, it can be useful to partition the overall active region into smaller active regions using quantum dots, quantum wires, or QWs (figure 3) to minimize the intraband collision time. Because the carrier collision rate for each partitioned active region is expected to become greater due to quantum confinement, which would yield a lower LWEF for the overall active region across which the beam propagation takes place, as will be shown later. It has indeed been shown by previous experimental studies that quantum confinement based SOAs display a smaller LWEF [18–21]. In the upcoming section we will investigate and explain why this decrease in the LWEF occurs in the case of quantum confinement, and the mechanism through which the partitioning of the active area using QWs influences the LWEF variation in relation to reduced intraband collision time.

2.2. Carrier lifetime

Another parameter that strongly affects the LWEF variation is the *carrier lifetime*. The carrier lifetime is computed by considering both radiative and nonradiative processes. The radiative recombination rate depends on the carrier density. As the carrier density increases, the radiative recombination rate increases linearly up to a very high degree of carrier concentration, thereby increasing the internal quantum efficiency. The nonradiative recombination rate may either depend weakly or very strongly on the carrier density according to the internal structure of the gain medium. The default nonradiative recombination mechanism is based on defect centers or impurities in the gain medium, which are usually independent of the carrier concentration. This is known as *trap-assisted recombination*.

When the carrier density is very high, nonradiative recombination starts to dominate over radiative recombination via *Auger recombination* and *leakage recombination*. These additional nonradiative recombination processes usually occur at a much lower rate unless the carrier density is very high. Leakage recombination in particular, is usually present for very thin, buried active regions such as QWs.

The Auger recombination is proportional to the cube of the carrier density and the leakage recombination is proportional to its power of 5.5 [44]. Since the homogenous broadening dominates over inhomogeneous broadening for SOAs [49, 50], the total interband transition linewidth can be computed as [44]

$$\gamma_{total} = \gamma_{radiative} + \gamma_{nonradiative} = A + BN + CN^2 + DN^{4.5} \quad (7)$$

$$\gamma_{trap} = A, \quad \gamma_{radiative} = BN, \quad \gamma_{Auger} = CN^2, \quad (8)$$

$$\gamma_{leakage} = DN^{4.5}$$

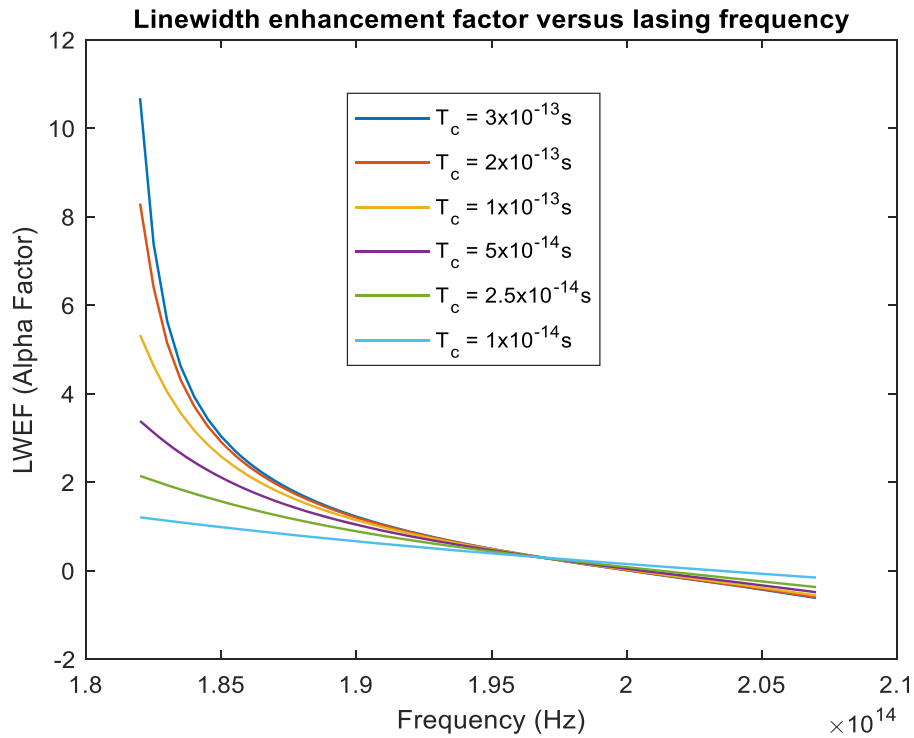


Figure 1. Plots of the LWEF against lasing frequency for various values of the intraband collision time T_c .

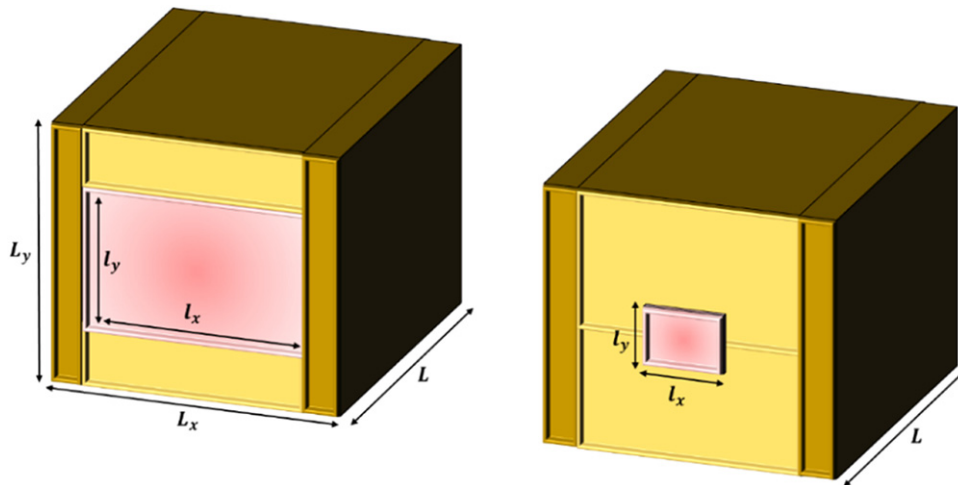


Figure 2. SOA with large/small active medium cross-section (active medium signified by light-red color).

where $A, B, C,$ and D are the recombination constants of a gain medium. The carrier lifetime is computed as

$$\tau_c = \frac{1}{\gamma_{total}} = \frac{1}{A + BN + CN^2 + DN^{4.5}}. \quad (9)$$

If the carrier density is not extremely high, the Auger and leakage recombination terms can be removed and the carrier lifetime can be approximated as

$$\tau_c = \frac{1}{\gamma_{total}} \approx \frac{1}{A + BN}, \quad \gamma_{total} \approx A + BN. \quad (10)$$

In gain media with low impurity concentrations, under moderately high carrier densities one can make the additional

assumption that

$$\gamma_{total} \approx BN, \quad \tau_c \approx \frac{1}{BN}. \quad (11)$$

In this case, radiative recombination becomes dominant, and the internal quantum efficiency is nearly equal to 1.

2.3. Computation of the LWEF

To compute the LWEF instantaneously via equations (2)–(4), one should start with the SOA rate equations to solve for the electron and hole concentrations, and then proceed to compute the instantaneous value of the refractive index, carrier lifetime, intraband collision time, and the photon lifetime within

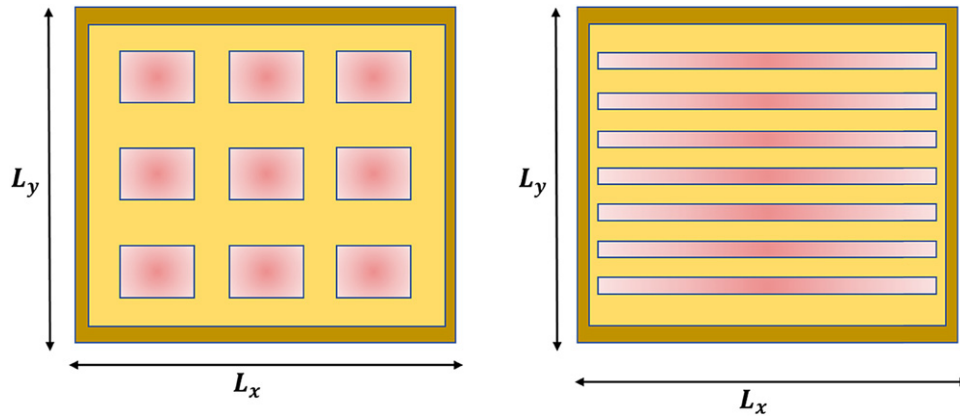


Figure 3. (a) An SOA cross-section with an active region that is based on multiple quantum-wires. (b) An SOA active region that is based on MQWs.

the cavity (figure 4). The initial electron/hole concentrations within the SOA WG are due to thermal excitation, which can be obtained from the intrinsic carrier concentration at room temperature.

As the electrons and holes are created in pairs, under electrical bias, their densities in time are given as

$$\eta(t) = \eta_0 + N(t), \quad \rho(t) = \rho_0 + N(t) \quad (12)$$

η_0 : initial electron density via thermal excitation

ρ_0 : initial hole density via thermal excitation

N : additional electron/hole density via electrical excitation.

An SOA active region can be of bulk-type or MQW-based. MQW SOAs are used for enhancing the confinement of electrons and photons within the active region, which consists of MQWs that are useful for capturing and trapping electrons via the potential difference that forms at their junction with the *barrier layers* that separate each well. The QW-barrier sequence is terminated by *separate confinement heterostructures* (SCHs) to enhance the optical confinement of the amplified beam. Figure 5 shows an MQW SOA active region that is sandwiched between the n-doped/p-doped cladding layers.

Given that the electrical excitation is strong enough, one can assume that $N(t) \gg \eta_0$, $N(t) \gg \rho_0$, therefore, throughout the analysis it is assumed that $\eta(t) = \rho(t) = N(t)$. To obtain the time variation of the electrically generated electron–hole pair concentration ($N(t)$), the subsequently outlined procedure is followed step by step:

2.3.1. Computation of the photon lifetime. The photon lifetime in an SOA active region changes based on the instantaneous value of the refractive index. The initial value of the refractive index can be chosen as the value in the dispersion-free range of the emission spectrum of the gain medium (e.g. 3.6 for GaAs)

$$\tau_p = \frac{n_r L}{c}, \quad \text{Photon lifetime} \quad (13)$$

L : length of the SOA active region, c : speed of light, n_r : refractive index.

2.3.2. Computation of the electron and photon densities in the active region. Using the rate equations for an SOA active layer (bulk or QW), the instantaneous electron and photon densities are computed for evaluating the instantaneous values of the carrier lifetime, photon lifetime, intraband collision time, and the refractive index (equations (14) and (15)) [42]

S : photon density, N : carrier density,

τ_p : photon lifetime, τ_c : carrier lifetime,

Γ : optical confinement factor

G : spectral small signal gain function,

ν_L : lasing frequency,

A_{cs} : cross sectional active medium area

Ω : gain linewidth, n : refractive index,

I : pump current, e : elementary charge

ν_0 : bandgap transition frequency, W : beam spot size,

λ : wavelength, d_{Ac} : active layer thickness

ξ_i : injection efficiency, d_{wg} : wave guide thickness,

ζ : optical power, h : Planck’s constant

τ_r : radiative recombination time,

n_{clad} : refractive index of the cladding,

\hbar : reduced Planck’s constant

n_{ac} : refractive index of the active region,

T_c : intraband collision time,

N_{th} : threshold carrier density

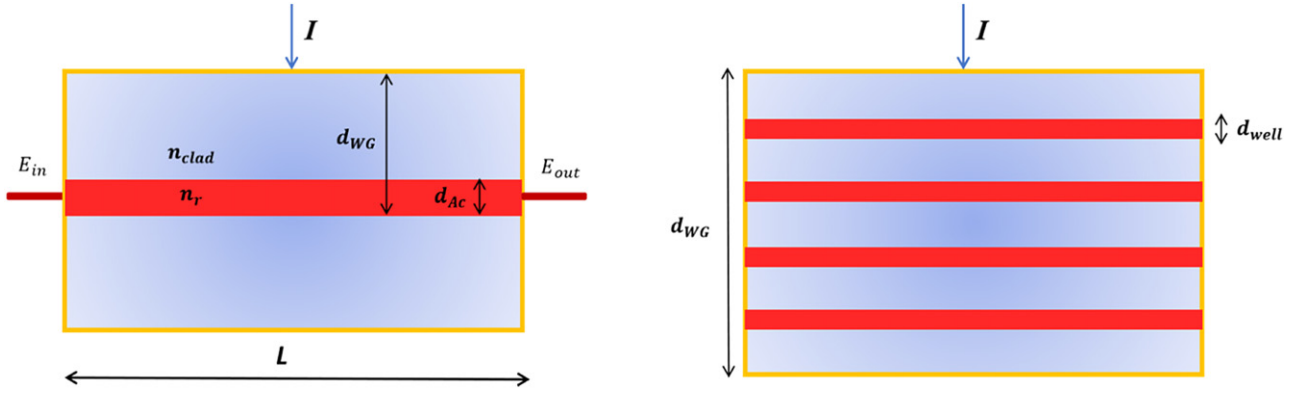


Figure 4. (a) Bulk SOA WG structure. The area in red signifies the electron confinement (active) region of the SOA, while the light-blue region signifies the cladding layer. The refractive index and the thicknesses of the active and cladding layers jointly determine the optical confinement ratio of the amplified laser beam. (b) MQW SOA where each well is a separate electron confinement region.

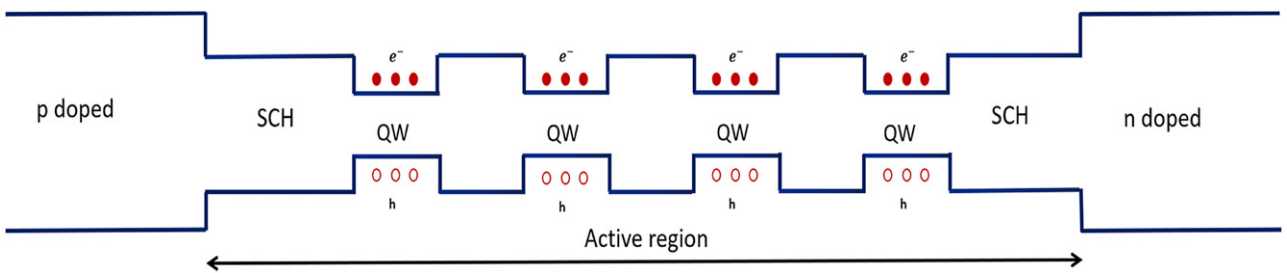


Figure 5. MQW SOA active region involving four QWs that are separated by barrier layers, followed by SCHs for enhanced optical confinement.

$$\frac{dN}{dt} = \frac{\xi I}{e A_{cs} L} - \frac{N}{\tau_c} - \Gamma(v_L) G(v_L) S \quad (14)$$

$$\frac{dS}{dt} = \Gamma(v_L) G(v_L) S - \frac{S}{\tau_p} + \frac{N}{\tau_r}, \quad \zeta = \frac{h v_L A_{cs} L}{\tau_p} S. \quad (15)$$

The gain function $G(v_L)$ in equations (14) and (15) has a Lorentzian dependence on the lasing frequency [49, 50]

$$G(v_L) = \frac{(N - N_{th}) \times \left(\frac{\lambda^2}{8\pi\tau_r}\right) \times (\Omega/2\pi) \times \left(\frac{c}{n_{ac}}\right)}{(v_L - v_0)^2 + (\Omega/2)^2}, \quad (16)$$

where $\Omega = (\frac{1}{\tau_c} + \frac{1}{T_c})$ is the gain linewidth and N_{th} is the threshold carrier density of the gain medium [50].

The optical confinement factor $\Gamma(v_L)$ depends on the beam spot size, ratio of the thickness of a given active region to the total WG thickness, and also to the refractive indices of the active and cladding regions. It is expressed as the ratio of the beam intensity in the active region to the total beam intensity in the WG [51]. Assuming a Gaussian intensity profile, the optical confinement factor is expressed as

$$\Gamma(v_L) = \frac{\int_{-z_1/2}^{z_1/2} n(z, v_L) \exp\left(-\left(\frac{z}{\sqrt{2}W}\right)^2\right) dz}{\int_{-z_0/2}^{z_0/2} n(z, v_L) \exp\left(-\left(\frac{z}{\sqrt{2}W}\right)^2\right) dz}, \quad \text{WG range: } \frac{-z_0}{2} < z < \frac{z_0}{2}, \quad \text{Active layer: } \frac{-z_1}{2} < z < \frac{z_1}{2}. \quad (17)$$

2.3.3. Computation of the instantaneous change in refractive index. In order to solve for the instantaneous values of the carrier lifetime, photon lifetime, and the intraband collision time, one needs to evaluate the change in the refractive index based on the instantaneous change in carrier density. To do this, the relative permittivity is updated by solving for the

real and imaginary parts of the electric susceptibility using equations (3) and (4). The real and imaginary susceptibility terms involve the computation of the density of states $\rho(E)$ and the conduction/valence band occupation probabilities $P_c(n, \omega)$ and $P_v(n, \omega)$. For bulk semiconductors, the density of states can be calculated using the following expressions [49]

$$\rho(E) = \frac{(2m_c)^{3/2}}{2\pi^2\hbar^3} \sqrt{E - E_c}, \quad E > E_c, \quad (18)$$

$$\rho(E) = \frac{(2m_v)^{3/2}}{2\pi^2\hbar^3} \sqrt{E_v - E}, \quad E_v > E$$

in which case, the energy level (E) is regarded as a continuous variable.

For SOAs with a MQW based active region, assuming that the wells are ideal and identical, based on the thickness of each well (d_1), E can only take the following values

$$\text{for MQWs: } E = E_c + E_q + E_{\text{kin}} = E_c + \frac{\hbar^2 q^2 \pi^2}{2d_1^2 m_c} + E_{\text{kin}},$$

$$q = 1, 2, 3, \dots \quad (19)$$

E_c : conduction band energy, m_c : electron effective mass

E_v : valence band energy, m_v : Hole effective mass.

In the case of QWs, the density of states is constant for each quantum number (q), and the total density of states can be stated as the sum of all densities of states via a staircase function

$$\rho(E) = \sum_{q=1}^{\infty} \frac{m_c}{\pi \hbar^2 d_1} u(E - E_q), \quad \text{where } u(E) \text{ is the unit step function.} \quad (20)$$

The conduction and valence band occupation probabilities are expressed as:

$$P_c(E) = \frac{1}{\exp\left(\frac{E - E_{fc}}{kT}\right) + 1} \quad (21)$$

$$P_v(E) = 1 - \frac{1}{\exp\left(\frac{E - E_{fv}}{kT}\right) + 1} \quad (22)$$

k : Boltzmann constant, T : temperature,

E_{fc} : conduction band Fermi level,

E_{fv} : valence band Fermi level.

2.3.4. Solve for the conduction and valence band Fermi energies (E_{fc}, E_{fv}) via an iterative rule. Once the carrier concentration is evaluated using the rate equations, the corresponding conduction and valence band Fermi levels are determined using any simple iterative method (such as the *Secant method*) according to the following root-finding problems

$$E_{fc} = \arg \min \left\{ \left| N - \int_{E_c}^{\infty} \rho(E) \frac{1}{\exp\left(\frac{E - E_{fc}}{kT}\right) + 1} dE \right| \right\} \quad (23)$$

$$E_{fv} = \arg \min \left\{ \left| N - \int_{-\infty}^{E_v} \rho(E) \left(1 - \frac{1}{\exp\left(\frac{E - E_{fv}}{kT}\right) + 1} \right) dE \right| \right\}. \quad (24)$$

2.3.5. Compute the LWEF. Finally, revisiting equations (2)–(4) and using equations (14)–(24), the LWEF can be computed as

$$\alpha(\omega_L, N, T_c) = - \frac{\int_{-\infty}^{\infty} \rho(\omega) \left[\frac{dP_c(N, \omega)}{dN} - \frac{dP_v(N, \omega)}{dN} \right] \frac{\omega_L - \omega}{(\omega_L - \omega)^2 + T_c^{-2}} d\omega}{\int_{-\infty}^{\infty} \rho(\omega) \left[\frac{dP_c(N, \omega)}{dN} - \frac{dP_v(N, \omega)}{dN} \right] \frac{T_c^{-1}}{(\omega_L - \omega)^2 + T_c^{-2}} d\omega}. \quad (25)$$

For the re-evaluation of each parameter at the next time-step, the value of the active layer refractive index $n_{ac} = n(-z_1/2 < z < z_1/2)$ is updated as

$$n_{ac} = \text{Re} \left\{ \sqrt{1 + \chi + \left\{ \frac{Ne^2}{m\epsilon_0} \right\}} \right\} \quad (26)$$

χ : background susceptibility,

ϵ_0 : free space permittivity, m : electron mass.

The modified value of the refractive index updates the confinement factor based on equation (17).

2.3.6. Computation of the carrier lifetime and the intraband collision time. As discussed in the previous subsection, the carrier lifetime and the intraband collision time are modified by the change in the carrier density of an active medium, which is represented by the relations

$$\tau_c = \frac{1}{\gamma_{\text{total}}} = \frac{1}{A + BN + CN^2 + DN^{4.5}},$$

$$T_c = \frac{C_1}{N} \quad (\text{For bulk SOAs}),$$

$$T_c = \frac{C_2}{N_{\text{QW}}} \quad (\text{For MQW SOAs})$$

N : carrier density, N_{QW} : QW carrier density,

C_1, C_2 : constants.

2.3.7. Parameter update and reiteration. Finally, each of the computed parameters at a given time step, is inserted back into the rate equations, and the whole procedure is repeated throughout the operation time of the SOA. After a certain duration, the SOA operation reaches a steady state and all parameters converge to certain values including the LWEF. In the upcoming computations, the steady state value of the LWEF will be computed for each given set of SOA parameters. For the sake of a simplified description of the whole process, figure 6 illustrates the summary of LWEF computation in terms of the aforementioned variables.

2.4. Active region carrier density versus QW carrier density

Concerning MQW SOAs, the active region consists of a sequence of QWs and adjacent barrier layers, which are altogether sandwiched between the SCHs. Some of the electrons are captured by the QWs while others tunnel through the barrier layers. This causes a sharp variation in the carrier density within the active region. Considering both the optical and the

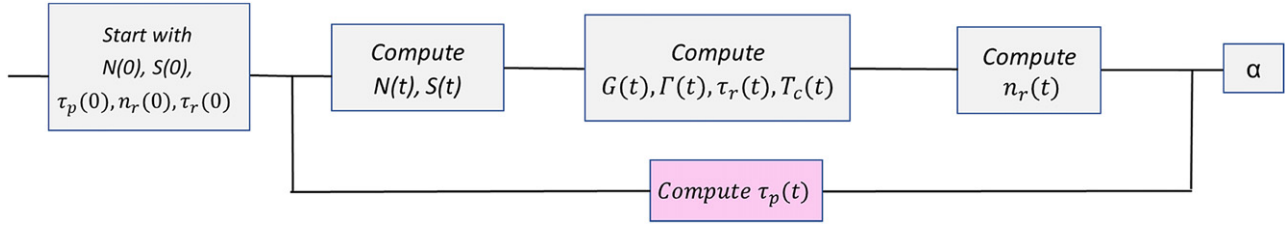


Figure 6. A simple illustration of the whole outlined process for LWEF computation.

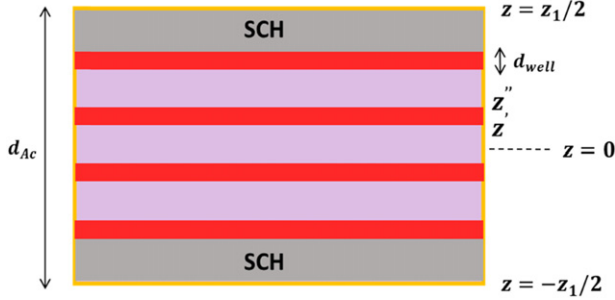


Figure 7. Active region of a MQW SOA. Red layers represent the wells and violet regions represent the barriers.

electron confinement within a single well, and also over the entire active region, the QW carrier density and the active region carrier density can be separately evaluated from the following rate equations [42, 52]

$$\frac{dN_{QW,i}}{dt} = \frac{\xi_i I}{eA_{cs,QW,i}L} - \frac{N_{QW,i}}{\tau_{c,QW}} - \Gamma_{QW,i}(v_L) G_{QW,i}(v_L) S_{QW,i} \quad (27)$$

$$\frac{dS_{QW,i}}{dt} = \Gamma_{QW,i}(v_L) G_{QW,i}(v_L) S_{QW,i} - \frac{S_{QW,i}}{\tau_p} + \frac{N_{QW,i}}{\tau_{r,QW}} \quad (28)$$

$$\frac{dN_{Ac}}{dt} = \frac{I}{eA_{cs}L} - \frac{N_{Ac}}{\tau_{c,Ac}} - \Gamma_{Ac}(v_L) G_{Ac}(v_L) S_{Ac} \quad (29)$$

$$\frac{dS_{Ac}}{dt} = \Gamma_{Ac}(v_L) G_{Ac}(v_L) S_{Ac} - \frac{S_{Ac}}{\tau_p} + \frac{N_{Ac}}{\tau_{r,Ac}} \quad (30)$$

In MQW SOAs with numerous wells, often most of the electrons are captured by the wells. Therefore, one can make the approximations $\tau_{c,Ac} \approx \tau_{c,QW}$, $\tau_{r,Ac} \approx \tau_{r,QW}$.

Here, one has to distinguish between the QW carrier density and the active region carrier density, due to the difference in the cross-sectional area ($A_{cs}, A_{cs,QW}$), electron confinement ratio (ξ_i), optical confinement factor ($\Gamma_{Ac}, \Gamma_{QW,i}$), and the small

signal gain ($G_{Ac}, G_{QW,i}$), where

$$\Gamma_{QW,i}(v_L) = \frac{\int_{z'}^{z''} n(z, v_L) \exp\left(-\left(\frac{z}{\sqrt{2W}}\right)^2\right) dz}{\int_{-z_0/2}^{z_0/2} n(z, v_L) \exp\left(-\left(\frac{z}{\sqrt{2W}}\right)^2\right) dz}, \quad (31)$$

$$\Gamma_{Ac}(v_L) = \frac{\int_{-z_1/2}^{z_1/2} n(z, v_L) \exp\left(-\left(\frac{z}{\sqrt{2W}}\right)^2\right) dz}{\int_{-z_0/2}^{z_0/2} n(z, v_L) \exp\left(-\left(\frac{z}{\sqrt{2W}}\right)^2\right) dz}$$

$$\text{Active layer: } \frac{-z_1}{2} < z < \frac{z_1}{2}, \quad \text{Well range: } z' < z < z'',$$

$$\text{Waveguide range: } \frac{-z_0}{2} < z < \frac{z_0}{2}$$

$$G_{QW,i}(v_L) = \frac{(N_{QW,i} - N_{th}) \times \left(\frac{\lambda^2}{8\pi\tau_r}\right) \times (\Omega/2\pi) \times \left(\frac{c}{n}\right)}{(v_L - v_0)^2 + (\Omega/2)^2},$$

$$G_{Ac}(v_L) = \frac{(N_{Ac} - N_{th}) \times \left(\frac{\lambda^2}{8\pi\tau_r}\right) \times (\Omega/2\pi) \times \left(\frac{c}{n}\right)}{(v_L - v_0)^2 + (\Omega/2)^2}. \quad (32)$$

When most of the electrons are captured by the wells, it can be assumed that the carrier density is nonzero only within the wells. This allows us to solve the rate equations only for the active region carrier density, and then infer about the QW carrier densities through the following relation

$$N_{Ac} \approx \frac{1}{d_{ac}} \sum_{i=1}^M N_{QW,i} d_i, \quad M : \text{number of wells}, \quad (33)$$

d_i : well width, d_{ac} : active layer thickness.

For MQW SOAs with identical wells, one can make the further approximation

$$N \approx N_{QW} \frac{M \times d_{well}}{d_{ac}}. \quad (34)$$

Equations (33) and (34) are useful in the computation of the LWEF of MQW SOAs, as the QW carrier density affects the intraband collision time and the active region carrier density affects the propagation of the optical beam. Based on equation (25) and the definition of the intraband collision time in equation (6), it can be concluded that in order to shrink the LWEF, an MQW SOA should be designed so that the QW carrier density is maximized and the active region carrier density is minimized (with an imposed lower bound by the intended

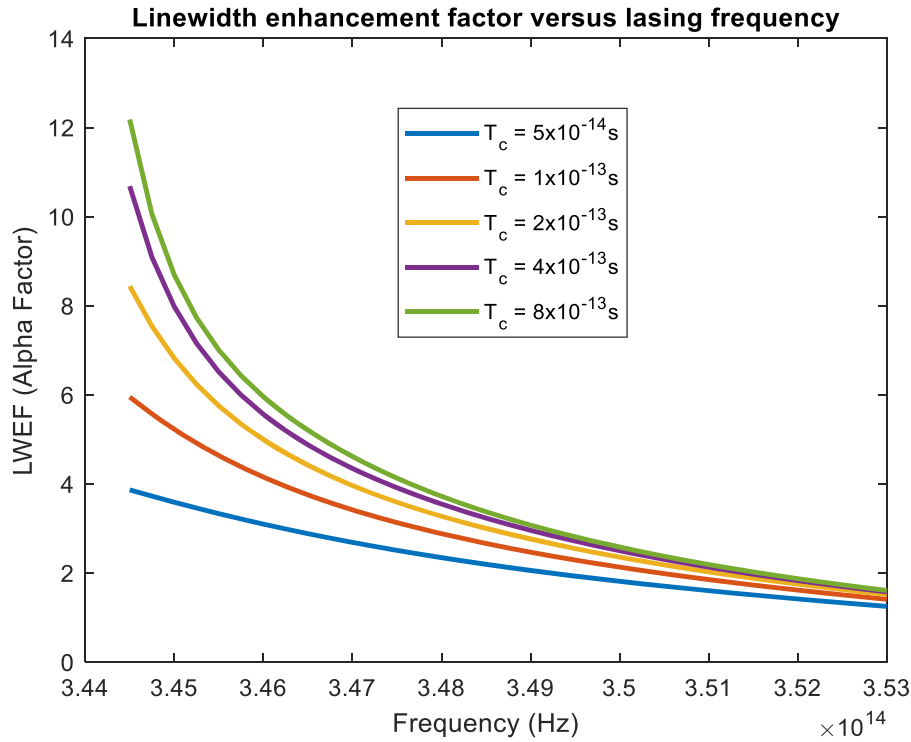


Figure 8. Variation of the LWEF against the lasing frequency for a bulk GaAs based SOA.

small-signal gain). As evident from equation (34), this necessitates the active medium design which employs the narrowest wells, and requires only a few wells for efficient electron confinement. Most importantly, equation (34) suggests that with MQW SOAs, one can have control over the LWEF through the engineering of the MQW structure (mainly the well widths), such that the QW carrier density is increased, and therefore the intraband collision time is decreased. For bulk SOAs however, as there is no electron confinement, one has little control on the LWEF (figure 7).

3. Results

3.1. The case of bulk SOAs

Firstly, a bulk GaAs based SOA with an undoped active layer is considered. The corresponding parameters for this SOA configuration are typically given as follows [44]

$$A_{cs} = 5 \times 10^{-13} \text{ m}^2, \quad I = 400 \text{ mA},$$

$$A = 13.5 \times 10^8 \text{ s}^{-1}, \quad n_{g0} = 3.6, \quad \Gamma_0 = 0.35$$

$$B = 5.6 \times 10^{-16} \text{ m}^3 \text{ s}^{-1},$$

$$C = 1.5 \times 10^{-40} \text{ m}^6 \text{ s}^{-1}, \quad D = 5 \times 10^{-100} \text{ m}^{13.5} \text{ s}^{-1}.$$

We will compare the results of our analysis with the experimental results in [39], which had investigated the variation of the LWEF for an undoped bulk GaAs–SOA at room temperature, under moderate pumping. The parameters of the SOA

that is used in the experiment are as given below

$$L = 0.3 \text{ mm}, \quad T_c = 0.2 \text{ ps}, \quad N_{th} = 1.55 \times 10^{24} / \text{m}^3,$$

$$E_{\text{bandgap}} = 1.424 \text{ eV}, \quad 344.5 \text{ THz} < \nu$$

$$< 353 \text{ THz (SOA bandwidth)}.$$

The intraband collision constant K is taken as 3×10^{11} , which yields the typical intraband collision time for a GaAs based SOA ($T_c = 0.2 \text{ ps}$) [39]. Using the procedure in section 2.3, based on all of the parameter values defined above, the LWEF is computed and plotted in figure 8 with respect to the lasing frequency (the yellow curve). The computation is repeated for the same SOA configuration for different collision times ($0.05 \text{ ps} < T_c < 0.8 \text{ ps}$) via tuning the constant K and keeping the carrier density as constant, as a hypothetical investigation. The LWEF is observed to be decreasing with a lowering of the intraband collision time. The computational results are in agreement with the theoretical and experimental results in [39] for a GaAs based undoped active layer within the gain bandwidth ($344.5 \text{ THz} < \nu < 353 \text{ THz}$). Here it is important to note that the practical value of the intraband collision time is rarely below 0.1 ps , unless the carrier density is drastically increased. The constant K depends on various factors, the most prominent being the SOA temperature. But it is practically very challenging if not impossible, to decrease K so sharply such that the intraband collision time gets below 0.1 ps and the LWEF can be considerably decreased further.

The intraband collision time is inversely affected from the variation of the carrier density as described in section 2.1.

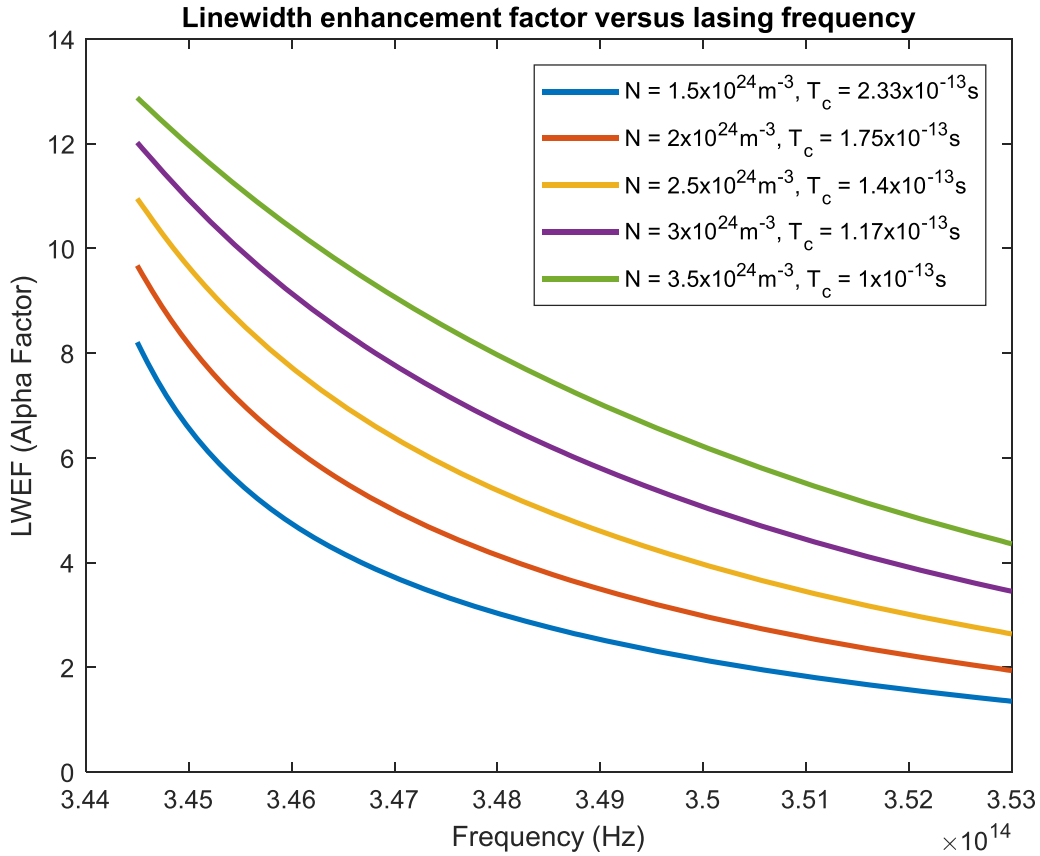


Figure 9. Variation of the LWEF for a bulk GaAs based SOA for different carrier densities.

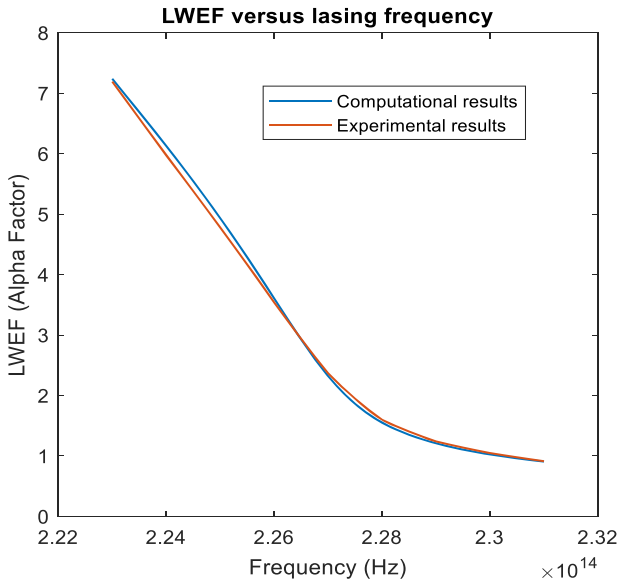


Figure 10. Computational and experimental LWEF values for the InP–InGaAsP MQW SOA.

Therefore, it is more meaningful to investigate its variation together with the corresponding variation of the carrier density in the SOA active region.

In practice, the intraband collision time can only be significantly tuned for a certain gain medium by changing the

carrier density within the active region, which can be controlled by tuning the pump current. After tuning the carrier density, it is observed that a decrease in the intraband collision time via an increase of the carrier density leads to a higher LWEF (see figure 9), which is the opposite of what was aimed. In figure 9, one can see that the LWEF attains the lowest values when the carrier density is minimum and the intraband collision time is maximum. As the carrier density is increased and the corresponding collision time is decreased, the values of the LWEF at each frequency steadily increases, eventually reaching to its maximum, for the highest carrier density and the associated minimum for the intraband collision time. This means that for bulk SOAs, the carrier density has a stronger effect on the LWEF compared to the intraband collision time. Obviously, the only way to decrease the LWEF for a bulk SOA, is to reduce the carrier density, which would restrict the SOA gain. Hence, for bulk SOAs, there is a trade-off between achieving a high SOA gain and the reduction of the LWEF.

3.2. Evaluating the LWEF for MQW SOAs

The LWEF of an MQW InP–InGaAsP SOA that is fabricated via liquid phase epitaxy growth technique, is investigated under room-temperature-based operating conditions and moderate optical pumping, according to its given experimental parameters and the corresponding results in [41]. The

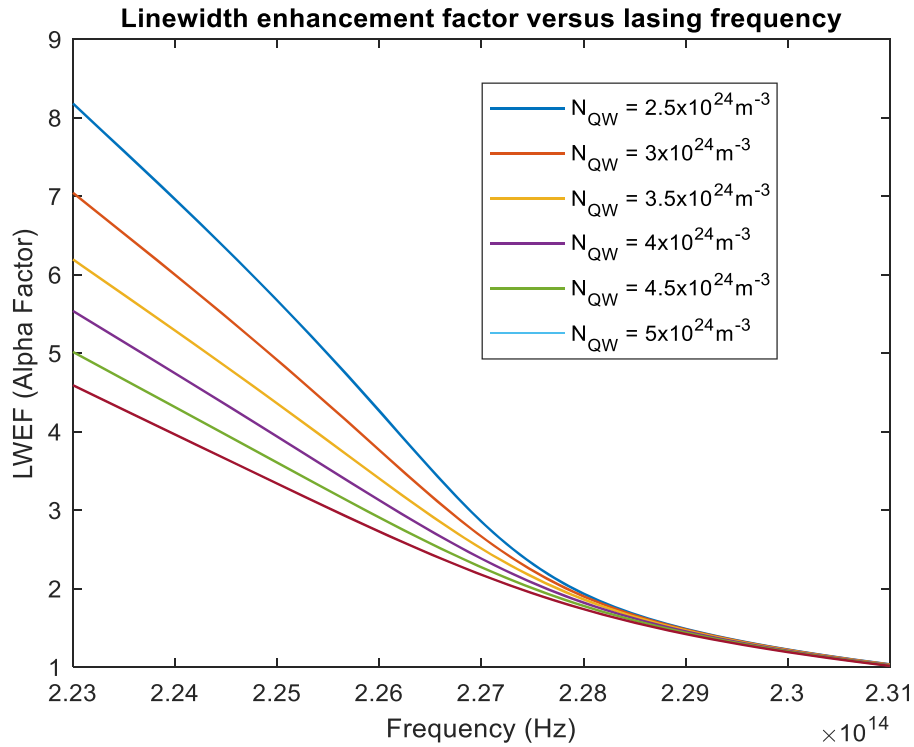


Figure 11. LWEF versus lasing frequency under various QW carrier densities for an MQW SOA with four wells and three barriers, each with a thickness of 15 nm.

experimental parameters of this SOA are given as [41]

$$d_{\text{well}} = 15 \text{ nm (Quantum well thickness),}$$

$$d_{\text{barrier}} = 15 \text{ nm (Barrier thickness),}$$

$$M = 4 \text{ (Number of wells),}$$

$$B = 3 \text{ (Number of barriers),}$$

$$A_{\text{cs, sheet}} = (d_{\text{well}}) \times (0.5 \times 10^{-6} \text{ m}),$$

$$d_{\text{active}} = 105 \text{ nm (Active layer thickness)}$$

$$N_{\text{th}} = 1.2 \times 10^{24} \text{ m}^{-3}, L = 0.25 \text{ mm,}$$

$$I = 0.15 \text{ A, } 223 \text{ THz} < \nu_L < 231 \text{ THz.}$$

The remaining parameters are chosen as typical SOA values that are provided in [44], which are given as

$$n_0 = 3.6, \quad \Gamma_0 = 0.35.$$

For an accurate comparison, these parameter values are also used in our computations. Assuming that the electrons are totally confined within the wells, the active region carrier density is computed via equations (29) and (30) as $N = 1.45 \times 10^{24} \text{ m}^{-3}$, and the corresponding QW carrier density is calculated based on equations (27) and (28) as $N_{\text{QW}} = 2.51 \times 10^{24} \text{ m}^{-3}$. The LWEF of the active region is obtained via equation (25). The computational results are shown in figure 10. They are in fair agreement with the experimental results in [41]. Part of the slight difference between the computational and experimental results might be due to the fact that the limits of the integrals in equation (25) go to infinity, yet we have taken the limits on the order of 10^{15} ,

beyond which there is very low contribution to the corresponding *Riemann sum* for both the numerator and the denominator. Other reasons for the difference might involve possible fluctuations of the optical confinement factor due to variations in the beam spot-size, and a slightly higher/lower intraband collision time due to a slightly higher/lower SOA temperature in the experiment.

Figure 11 illustrates the scenario, where the pump current and the active region length are simultaneously increased (at the same proportion). However, the well widths and the number of wells are kept constant to increase the QW carrier density based on equation (34). Consequently, the carrier density of the active region remains relatively constant, but the QW carrier density increases proportionally. This increase in the QW carrier density (N_{QW}) leads to a corresponding decrease in the intraband collision time and the LWEF. The coinciding variation of the LWEF with respect to the QW carrier density is illustrated in figure 11. Here, one can see that the LWEF is maximum at a given frequency for the lowest value of the QW carrier density. As the QW carrier density increases, the corresponding LWEF decreases for an arbitrary frequency. The LWEF is maximum for the lowest frequency within the gain-bandwidth (which is around the transition frequency) and gradually decreases for higher frequencies. Beyond a certain frequency within the gain-bandwidth, the LWEF attains a single value for all QW carrier densities and eventually converges to 1 for the given parameters.

The computation is repeated for an arbitrary MQW SOA with a longer active region and with fewer wells, this time

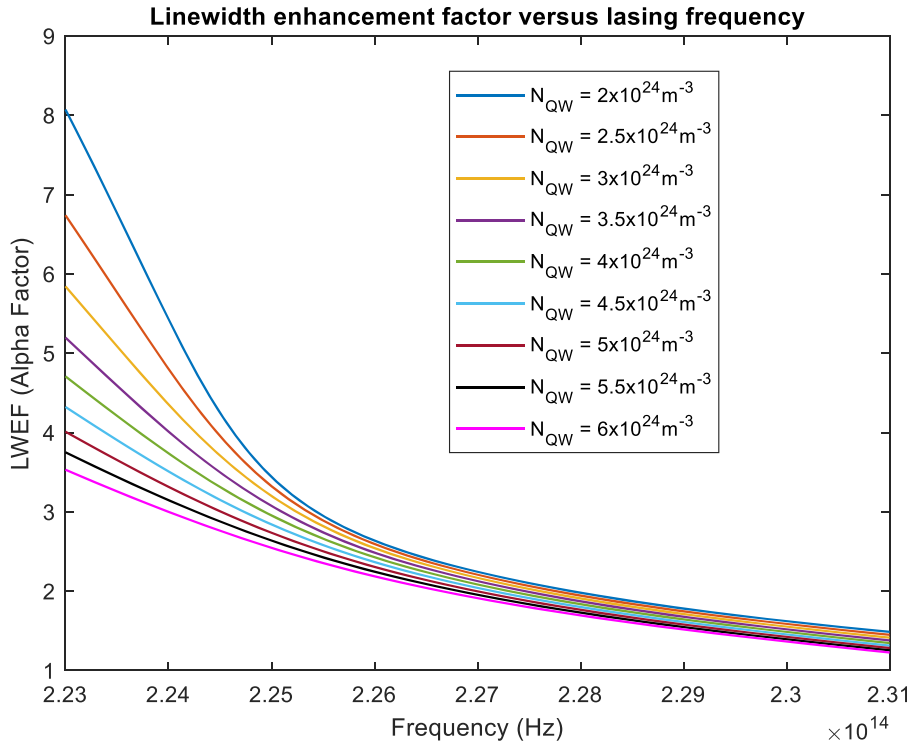


Figure 12. LWEF vs lasing frequency for various well carrier densities of an MQW SOA with three wells.

under the parameters given below

$$d_{\text{well}} = 20 \text{ nm}, \quad d_{\text{barrier}} = 25 \text{ nm}, \quad M = 3,$$

$$N_{\text{active}} = 1.3 \times 10^{24} \text{ m}^{-3},$$

$$B = 2, \quad d_{\text{Ac}} = 250 \text{ nm} \quad (\text{Active region length})$$

$$A_{\text{cs,well}} = (d_{\text{well}}) \times (10^{-6} \text{ m}),$$

$$N_{\text{th}} = 1.1 \times 10^{24} \text{ m}^{-3}, \quad L = 0.3 \text{ mm},$$

$$n_{g0} = 3.6, \quad \Gamma_0 = 0.3, \quad 223 \text{ THz} < \nu_L < 231 \text{ THz}.$$

The resulting variation of the LWEF is shown in figure 12. A decrease in the LWEF is evident for higher N_{QW} . Once again it is observed that the LWEF gradually decreases for higher frequencies within the gain-bandwidth and the difference between each LWEF value (at a certain frequency), corresponding to each QW carrier density, gradually decreases as the frequency is increased. The maximum value of the LWEF is 8 for a QW carrier density of $2 \times 10^{24} \text{ m}^{-3}$. Notably, it decreases to 3.5 under a QW carrier density of $6 \times 10^{24} \text{ m}^{-3}$. Based on this variation of the LWEF, it can be projected that the LWEF can be further decreased to super-low values for QW carrier densities on the order of 10^{25} m^{-3} under ultra-thin well thicknesses. In fact, a maximum LWEF value below 2 has been suggested to prevent significant noise formation in frequency-swept lasers where the frequency variation of the LWEF is of critical importance [27]. Hence, this study indicates the importance of employing MQW based SOAs with ultra-thin well thicknesses in frequency-swept lasers, to improve the signal to noise ratio and to prevent the formation of unwanted artifacts and instabilities in the output laser signal pattern. This

can greatly improve the quality of imaging and detection in many applications.

Figures 11 and 12 show that higher QW carrier densities enable the attainment of lower LWEFs. Therefore, an MQW SOA can be designed to operate at a relatively high active medium carrier density (thereby offering higher small signal gain), while inducing low-level refractive index fluctuations. This is achievable in MQW SOAs as most carriers can be confined within narrow QWs, so that the intraband collision rate can be maximized and the resulting LWEF is minimized for a given set of parameters in the design stage.

4. Conclusion

For an SOA with a bulk active region, one has little to no control on refractive index fluctuations, which occur naturally within the gain bandwidth of an SOA active layer. Although a high carrier density is desirable for improved small signal gain, this makes bulk SOAs susceptible to a high LWEF, which is often aggravated by a low carrier collision rate via stronger phase distortions. Since the intraband collision rate and the carrier density are completely interdependent in a bulk SOA, these parameters are not separately tunable, and the only way to reduce the LWEF in a bulk SOA is to decrease the carrier density, thereby compromising the SOA gain.

MQW SOAs enable the confinement of electrons within narrow wells. By designing MQW SOAs that operate under relatively large pump currents, and have relatively longer active layers, one can achieve a higher optical gain. Yet, for a given active layer carrier density, if most of the electrons in the active region are confined within the ultra-narrow wells, the

QW carrier density can be engineered to become quite high and the corresponding intraband collision rate can be maximized. This yields to a sharp decrease in the LWEF, which quantifies the refractive index fluctuations within the active region. The ideal scenario is to design an MQW SOA with a large optical confinement region that employs only a few wells, which are ultra-narrow in thickness and have a high electron confinement ratio, that enable an efficient confinement of all the electrons within the active region. This way, a high optical gain and a low LWEF can be simultaneously achieved.

Data availability statement

The data are available within the article.

Code availability

Available from the author upon reasonable request.

Conflict of interest

On behalf of all authors, the corresponding author states that there is no conflict of interest.

Funding statement

This research received no external funding.

ORCID iDs

Özüm Emre Aşırım  <https://orcid.org/0000-0003-0531-401X>

Christian Jirauschek  <https://orcid.org/0000-0003-0785-5530>

References

- [1] Paschotta R 2008 Linewidth enhancement factor *Encyclopedia of Laser Physics and Technology* 1st edn (New York: Wiley)
- [2] Quimby R 2006 *Photonics and Lasers* (New York: Wiley) pp 185–215
- [3] Huber R, Wojtkowski M and Fujimoto J 2006 Fourier domain mode locking (FDML): a new laser operating regime and applications for optical coherence tomography *Opt. Express* **14** 3225
- [4] Mazzucato S *et al* 2015 Gain, amplified spontaneous emission and noise figure of bulk InGaAs/InGaAsP/InP semiconductor optical amplifiers *IET Optoelectron.* **9** 52–60
- [5] Piprek J, Bjorlin E S and Bowers J E 2001 Optical gain-bandwidth product of vertical-cavity amplifiers *Technical Digest, Summaries of Papers Presented at the Conf. Lasers and Electro-Optics, Postconference Technical Digest (IEEE Cat. No. 01CH37170)* p 111
- [6] Qasaimeh O 2018 Multichannel and multistate all-optical switch using quantum-dot and sample-grating semiconductor optical amplifier *Electronics* **7** 166
- [7] Xiao J and Huang Y 2008 Numerical analysis of gain saturation, noise figure, and carrier distribution for quantum-dot semiconductor-optical amplifiers *IEEE J. Quantum Electron.* **44** 448–55
- [8] Chuang C, Liao Y, Lin C, Chen S, Grillot F and Lin F 2014 Linewidth enhancement factor in semiconductor lasers subject to various external optical feedback conditions *Opt. Express* **22** 5651
- [9] Spitz O, Herdt A, Duan J, Carras M, Elsässer W and Grillot F 2019 Extensive study of the linewidth enhancement factor of a distributed feedback quantum cascade laser at ultra-low temperature *Proc. SPIE, Quantum Sensing and Nano Electronics and Photonics XVI* vol 10926 p 1092619
- [10] Ruan Y, Liu B, Yu Y, Xi J, Guo Q and Tong J 2018 Measuring linewidth enhancement factor by relaxation oscillation frequency in a laser with optical feedback *Sensors* **18** 4004
- [11] Harder C, Vahala K and Yariv A 1983 Measurement of the linewidth enhancement factor α of semiconductor lasers *Appl. Phys. Lett.* **42** 328–30
- [12] Opacak N, Dal Cin S, Hillbrand J, Strasser G and Schwarz B 2021 Origin of the linewidth enhancement factor: resonant processes behind optical frequency comb formation *Proc. SPIE, Novel In-Plane Semiconductor Lasers XX* vol 11705 p 1170511
- [13] Fan Y, Yu Y, Xi J, Rajan G, Guo Q and Tong J 2015 Simple method for measuring the linewidth enhancement factor of semiconductor lasers *Appl. Opt.* **54** 10295
- [14] Yuan Z, Wang H, Wu L, Gao M and Vahala K 2020 Linewidth enhancement factor in a microcavity Brillouin laser *Optica* **7** 1150
- [15] Chattopadhyay T, Bhattacharyya P and Ghosh C 2015 Linewidth enhancement factor measurement of a Fabry Perot laser diode through narrowband optical FM generation *J. Opt. Commun.* **38** 141–5
- [16] Ukhanov A *et al* 2002 Orientation dependence of the optical properties in InAs quantum-dash lasers on InP *Appl. Phys. Lett.* **81** 981–3
- [17] Al-Khursan A H 2008 Linewidth enhancement factor in the quantum dots: non-thermal coupling case *Recent Pat. Electr. Eng.* **1** 84–8
- [18] Miloszewski J, Wartak M, Weetman P and Hess O 2009 Analysis of linewidth enhancement factor for quantum well structures based on InGaAsN/GaAs material system *J. Appl. Phys.* **106** 063102
- [19] Ohtoshi T and Chinone N 1989 Linewidth enhancement factor in strained quantum well lasers *IEEE Photonics Technol. Lett.* **1** 117–9
- [20] Holzinger S *et al* 2018 Determining the linewidth enhancement factor via optical feedback in quantum dot micropillar lasers *Opt. Express* **26** 31363
- [21] Zhang Z, Jung D, Norman J, Chow W and Bowers J 2019 Linewidth enhancement factor in InAs/GaAs quantum dot lasers and its implication in isolator-free and narrow linewidth applications *IEEE J. Sel. Top. Quantum Electron.* **25** 1–9
- [22] Ri C, Kim C, Oh Y and Kim S 2020 Immediate estimation of feedback factor and linewidth enhancement factor from measured self-mixing signals under moderate or strong regime *Meas. Sci. Technol.* **31** 065204
- [23] Yamada N, Hirata T, Maeda M and Hosomatsu H 1989 Basic properties, linewidth enhancement factor and spectral linewidth of SQW laser diodes emitting in the 780 nm region *Japan. J. Appl. Phys.* **28** L2219–21
- [24] Haug H and Haken H 1967 Theory of noise in semiconductor laser emission *Z. Phys. A* **204** 262–75
- [25] Henry C 1982 Theory of the linewidth of semiconductor lasers *IEEE J. Quantum Electron.* **18** 259–64
- [26] Schmidt M, Grill C, Lotz S, Pfeiffer T, Huber R and Jirauschek C 2021 Intensity pattern types in broadband Fourier domain mode-locked (FDML) lasers operating beyond the ultra-stable regime *Appl. Phys. B* **127** 60

- [27] Schmidt M, Pfeiffer T, Grill C, Huber R and Jirauschek C 2020 Self-stabilization mechanism in ultra-stable Fourier domain mode-locked (FDML) lasers *OSA Contin.* **3** 1589
- [28] Grillot F *et al* 2020 Physics and applications of quantum dot lasers for silicon photonics *Nanophotonics* **9** 1271–86
- [29] Kano F, Yoshikuni Y, Fukuda M and Yoshida J 1991 Linewidth enhancement factor of 1.3 μm InGaAsP/InP strained-layer multiple-quantum-well DFB lasers *IEEE Photonics Technol. Lett.* **3** 877–9
- [30] Dagens B *et al* 2005 Giant linewidth enhancement factor and purely frequency modulated emission from quantum dot laser *Electron. Lett.* **41** 323
- [31] Paul R, Summers H, White I, Rees P, Blood P, Rees P and Summers H 1994 Reduction of linewidth enhancement factor in strained 1.55 μm InGaAsP lasers *Conf. Lasers and Electro-Optics Europe—Technical Digest*
- [32] Yan S 2018 Dynamic characteristics in an external-cavity multi-quantum-well laser *Chin. Phys. B* **27** 060501
- [33] Zubov F *et al* 2015 Observation of zero linewidth enhancement factor at excited state band in quantum dot laser *Electron. Lett.* **51** 1686–8
- [34] Szwaj C, Lacot E and Hugon O 2004 Large linewidth-enhancement factor in a microchip laser *Phys. Rev. A* **70** 033809
- [35] Kim K C, Yoo Y C, Jung J H, Jeong J W, Han I K, Lee J I, Kim D H and Kim T G 2007 Investigation of linewidth enhancement factor for two types of quantum dot laser diode *Conf. Lasers and Electro-Optics/Pacific Rim, CLEOPR (Optics InfoBase Conf. Papers)* (Optical Society of America)
- [36] Soldo M *et al* 2013 Different values for the linewidth enhancement factor of a quantum-dots laser obtained using optical and electrical modulation *Conf. Lasers & Electro-Optics Europe & Int. Quantum Electronics Conf. CLEO EUROPE/IQEC*
- [37] Yang W 2010 Linewidth enhancement factor simplified *Proc. IEEE SoutheastCon* pp 305–7
- [38] Tan C, Wang Y, Djie H and Ooi B 2009 The dynamic characteristics and linewidth enhancement factor of quasi-supercontinuum self-assembled quantum dot lasers *IEEE J. Quantum Electron.* **45** 1177–82
- [39] Vahala K, Chiu L, Margalit S and Yariv A 1983 On the linewidth enhancement factor α in semiconductor injection lasers *Appl. Phys. Lett.* **42** 631–3
- [40] Aşırım Ö 2021 Far-IR to deep-UV adaptive supercontinuum generation using semiconductor nano-antennas via carrier injection rate modulation *Appl. Nanosci.* **12** 1–16
- [41] Green C, Dutta N and Watson W 1987 Linewidth enhancement factor in InGaAsP/InP multiple quantum well lasers *Appl. Phys. Lett.* **50** 1409–10
- [42] Huang Y-Z 1995 On the rate equations of semiconductor lasers for measuring spontaneous emission factor *IEEE Photonics Technol. Lett.* **7** 977–9
- [43] McLean T and Paige E 1960 A theory of the effects of carrier–carrier scattering on mobility in semiconductors *J. Phys. Chem. Solids* **16** 220–36
- [44] Wang J, Maitra A, Poulton C, Freude W and Leuthold J 2007 Temporal dynamics of the alpha factor in semiconductor optical amplifiers *J. Lightwave Technol.* **2** 891–900
- [45] Inan U S and Gołkowski M 2011 *Principles of Plasma Physics for Engineers and Scientists* (Cambridge: Cambridge University Press) pp 64–80
- [46] Haberland H, Bonitz M and Kremp D 2001 Harmonics generation in electron–ion collisions in a short laser pulse *Phys. Rev. E* **64** 026405
- [47] Goodnick S and Lugli P 1988 Effect of electron–electron scattering on nonequilibrium transport in quantum-well systems *Phys. Rev. B* **37** 2578–88
- [48] Leyland W *et al* 2007 Enhanced spin-relaxation time due to electron–electron scattering in semiconductor quantum wells *Phys. Rev. B* **75** 165309
- [49] Saleh B E A and Teich M C 2019 *Fundamentals of Photonics* 3rd edn (New York: Wiley) pp 645–789
- [50] Silfvast W T 2004 *Laser Fundamentals* 2nd edn (Cambridge: Cambridge University Press) pp 89–109 & 578–579
- [51] Huang Y, Pan Z and Wu R 1996 Analysis of the optical confinement factor in semiconductor lasers *J. Appl. Phys.* **79** 3827
- [52] Agrawal G P 2007 *Fiber-Optic Communication Systems* 3rd edn (New York: Wiley) pp 78–118